WATER EQUIVALENT THICKNESS ESTIMATION VIA SPARSE DECONVOLUTION OF PROTON RADIOGRAPHY DATA

Sylvain Deffet[⋆]*, Benoît Macq*[⋆]*, François Vander Stappen*[†] *and Paolo Farace*[‡]

[⋆]ICTEAM, Université catholique de Louvain, Louvain-La-Neuve, 1348, Belgium
[†]Ion Beam Applications (IBA), Louvain-La-Neuve, 1348, Belgium
[‡]Proton Therapy Unit, Hospital of Trento, Trento, 38122, Italy

ABSTRACT

Proton radiography using a multilayer ionization chamber can potentially be used for assessing the quality of the stopping power computation in proton therapy. However, the finite proton beam profile leads to a degradation of the depth-dose curves ('blurring') measured by the range probe, which makes the estimation of the integrated proton stopping power a complex task. Existing methods aiming at determining a map of the integrated proton stopping power currently involve the use of the planning x-ray computed tomography (CT) as a priori knowledge. Consequently, such methods are very sensitive to small misalignment between the planning CT and the proton radiography acquisitions, to errors in the stopping power computation and to changes in the anatomy of the patient. In this paper, we develop an algorithm based on a sparsity assumption that estimates the integrated proton stopping power map of an anthropomorphic phantom from proton radiography data without using any prior information from the CT.

Index Terms— Proton Radiography, Particle Imaging, Range Uncertainty, Multi Layer Ionization Chamber, Deconvolution

1. INTRODUCTION

The advantage of proton therapy over conventional radiation therapy relies on the fact that protons deliver a sharp dose at a precise location known as the Bragg peak. Unfortunately, the conversion from the Hounsfield Units (HU) of the planning CT to relative proton stopping powers (RSP) is tainted by uncertainties which usually lead physicians to choose to irradiate an area larger than theoretically needed [1].

Proton radiography has benefited from a recent body of research which demonstrated its clinical potential to better quantify and potentially reduce the range uncertainty [2, 3]. In particular, it offers the potential to generate patient-specific conversion curve from HU to RSP by combining a map of integrated RSP with the planning x-ray CT [4, 5, 6].

Proton radiography with a multilayer ionization chamber consists in scanning through a phantom and recording the pairs consisting of the position of each of the pencil beam shots and its corresponding measured integral depth-dose profiles (IDD), examples of which are shown in Fig. 1.

Because the shapes of the IDD are impacted by the transit of protons through lateral heterogeneities in a process called range mixing, one can not directly determine the integrated RSP also referred to as water equivalent thickness (WET), from the measurements. Two approaches currently exist. On the one hand, Farace et al [3] implemented the idea proposed by Mumot et al [7] of performing a comparison between the IDD measured by the MLIC with those simulated by a treatment planning system. On the other hand, Krah et al [8] proposed to decompose each IDD into a set of pristine Bragg curves from which the WET would be directly obtained. To spatially distribute the WET determined by the decomposition, the use of a WET map estimated from the planning CT was shown to improve greatly the results of a demosaicing step based on the radiography data only.

However, the use of the planning CT in the two methods makes them sensitive to errors in the RSP computation and to residual set-up errors. The WET map estimate could also be altered by changes in the anatomy of the patient and relative displacements of moving organs that could take place between the CT acquisition and the proton radiography.

In this paper, we show that under the assumption that the WET map has a sparse representation, it can be obtained without using any prior knowledge derived from the planning CT. In section 2, an iterative algorithm is built to perform a deconvolution of the IDD and to increase the spatial resolution of the WET map. In section 3, the method is applied to both synthetic data and actual proton radiography acquisitions.

2. MATERIALS AND METHODS

2.1. IDD Simulation

As experimentally demonstrated by Farace et al [9] the measured IDD consists of a convolution of a Gaussian kernel G having a standard deviation equal to the spot size with shifted versions of a pristine Bragg curve, called IDD_{ref}, which corresponds to the IDD that would be

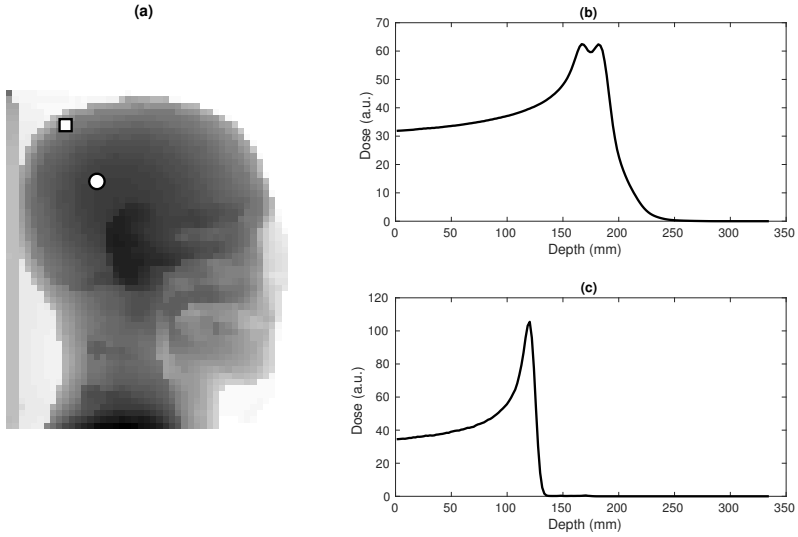

Fig. 1. (a) Projection in the form of a range map of a proton radiograph obtained with a gantry angle of 270° and examples of the IDD underlying each pixel such as (b) the one corresponding to the square dot and (c) the one corresponding to the round dot.

measured without the phantom through the beam path:

$$\begin{aligned} IDD(x_i, y_i, z) &= \sum_{j \in S_i} G(x_i - x_j, y_i - y_j) \\ & \quad IDD_{ref}(z + WET(x_i, y_i)) \end{aligned} \quad (1)$$

where (x_i, y_i) are the coordinates of each pencil beam, z refers to the depth axis of the IDD, WET refers to the water-equivalent thickness of the phantom along the path of the beam and S_i denotes the set of the indices of the pixels lying in the cross-section of the beamlet. In the case of parallel beamlets, the WET can be estimated from the HU of the planning CT via

$$WET(x, y) = \sum_z RSP(HU(x, y, z)) s_z \quad (2)$$

where RSP is usually a piecewise linear function associating to each HU the RSP, and s_z is the size of a voxel along the z-direction.

2.2. Deconvolution

For clarity, we consider a matrix formulation of the equations. In this matrix format, Eq. 1 becomes:

$$\boldsymbol{IDD_{meas}}(z) \approx \boldsymbol{G}\, \boldsymbol{IDD_r}(z\mathbb{1} + \boldsymbol{WET}) \quad (3)$$

where $\boldsymbol{G}$ is the circulant matrix associated with the convolution kernel G and $\boldsymbol{IDD_r}$ is defined by

$$IDD_{r,i}(z) = IDD_{ref}(z) \quad (4)$$

We consider a transform $\boldsymbol{\Psi}$ such that the WET can be represented through the coefficients $\boldsymbol{\alpha}$:

$$\boldsymbol{WET} = \boldsymbol{\Psi\alpha} \quad (5)$$

In this study, $\boldsymbol{\Psi}$ is the matrix associated with an inverse wavelet transform.

Under sparsity assumptions, one could recover the WET by solving the problem

$$\begin{aligned} \boldsymbol{\alpha}^\star &= \arg\min_{\boldsymbol{\alpha}} ||\boldsymbol{\alpha}||_0 \\ & \text{s.t.} \quad f_1(\boldsymbol{\alpha}) \leq \epsilon \end{aligned} \quad (6)$$

where the function $f_1(\boldsymbol{\alpha})$ is a similarity measure between the measured data and the model consisting of Eq. 3 and 5:

$$\begin{aligned} f_1(\boldsymbol{\alpha}) = \int_0^{l_d} & ||\boldsymbol{IDD_{meas}}(z) \\ & - \boldsymbol{G}\, \boldsymbol{IDD_r}(z\mathbb{1} + \boldsymbol{\Psi\alpha})||_2^2 \, dz \end{aligned} \quad (7)$$

Relaxing Eq. 6 with a l_1 norm and assuming that f_1 is convex, the minimization problem can be solved with the proximal method which provides an iterative algorithm:

$$\boldsymbol{\alpha_{n+1}} = \text{prox}_{\gamma, f_2}\left(\boldsymbol{\alpha_n} - \gamma \nabla f_1(\boldsymbol{\alpha_n})\right) \quad (8)$$

with

$$f_2(\lambda, \boldsymbol{\alpha}) = \frac{1}{2\lambda} ||\boldsymbol{\alpha}||_1 \quad (9)$$

The following expression was used for ∇f_1:

$$\nabla f_1(\boldsymbol{\alpha}) = 2\boldsymbol{\Psi}^T \int_0^{l_d} (\boldsymbol{DIDD_r}(z\mathbb{1} + \boldsymbol{\Psi\alpha})$$

$$\circ (\boldsymbol{G}\ (\boldsymbol{G}\,\boldsymbol{IDD_r}(z\mathbb{1}+\boldsymbol{\Psi\alpha}) - \boldsymbol{IDD_{meas}}(z)))\,dz \qquad (10)$$

where $\boldsymbol{DIDD_r}$ is defined by:

$$DIDD_{r,i}(z) = \frac{d}{dx} IDD_{ref}(x)\bigg|_{x=z} \qquad (11)$$

and was computed by finite difference.

To increase the spatial resolution, a downsampling operator was added into Eq. 3:

$$\boldsymbol{IDD_{meas}}(z) \approx \boldsymbol{D\,G\,IDD_r}(z\mathbb{1}+\boldsymbol{WET}) \qquad (12)$$

and Eq. 7 and the expression of its gradient were adapted accordingly.

2.3. Proton Radiographs Simulations and Actual Measurements

The deconvolution was applied to both actual measurements performed with the commercial MLIC named Giraffe (IBA Dosimetry, Belgium) and to simulated proton radiographs which provide a ground truth to compare the results with.

The analytical model introduced in section 2.1 was used to generate the simulated proton radiographs from a CT scan of an anthropomorphic head phantom (CIRS, USA). Additive noise similar to the one used by Deffet et al [10] for the robustness analysis of a registration method for proton radiography data was added to the simulated proton radiographs.

The actual proton radiographs were acquired with the Giraffe after an accurate kV-kV alignment of the head phantom on the treatment couch. As for the investigation of the Giraffe for proton radiography [9, 10], the proton beam was characterized by a spot size of 3 mm (one sigma), an energy of 210 MeV, a spot spacing of 5 mm and the beamlets were considered as being parallel.

3. RESULTS AND DISCUSSION

The conversion from HU to RSP is one of the major contributions to the range uncertainty in proton therapy [1]. Proton radiography seems to be a promising tool for assessing the RSP computation thanks to its ability to provide range error maps obtained by a comparison with values based on the planning CT.

The proposed WET estimation method was applied to proton radiographs obtained with a spot spacing of 5 mm, a value used by other authors for particle imaging [8, 3]. A projection in the form of a range map of a simulated proton radiograph is shown in Fig. 2b. The true WET is depicted in Fig. 2a with pixels of size 1x1 mm. The WET map obtained by the application of the proposed deconvolution technique is shown in Fig. 2c. The spatial resolution was increased by 5 along each direction leading to pixels of size 1x1 mm.

In proton therapy, the contribution of the RSP computation to the range uncertainty is usually expressed in terms of relative errors and is expected to be around 3.5% [1]. The map of relative error between the optimized WET and the ground truth is shown in Fig. 2d. Areas consisting only of air which does not contribute significantly to the range uncertainty were overwritten with black pixels. Omitting those areas, the mean relative error was 1.1%. The largest errors appear to be mostly localized on sharp transitions. This should be accounted for if the WET-map is later used for optimizing the conversion curve from HU to RSP. To do so, an intriguing option could be the use of a heterogeneity index such as the one proposed by Pflugfelder et al, in order to define regions of interest [11].

The proposed method was also applied to real measurements as shown in Fig. 3. On Fig. 3c, the WET map obtained from the acquired proton radiograph was compared with the one estimated by our treatment planning system. First, the error on the skull, at the interface with the air, seems to suggest that there remained a residual misalignement between the CT and the acquired proton radiograph, despite the accurate kV-kV alignment. The application in post-processing of the registration method proposed by Deffet et al [10] significantly decreased this error, as can be seen in Fig. 3d. Secondly, the similarities between Fig. 2c and Fig.3b and between Fig. 2d and Fig. 3d suggest that the method worked equally well on real data and simulated ones. Fig. 3d is a striking example of the benefit of generating such high resolution WET maps as it clearly appears that the RSP of the titanium implant was wrongly estimated and the conversion curve to RSP could accordingly be corrected.

4. CONCLUSION

In this paper, we have developed an algorithm to estimate the WET map of an anthropomorphic phantom from proton radiography data without using any prior information from the CT. Consequently, the results are not impacted by residual set-up errors, wrong RSP computation nor changes in the anatomy of the patient. In the results section, WET maps with pixels of 1x1 mm were obtained from proton radiographs acquired with a spot spacing of 5 mm. The mean relative error was 1.1%.

Such a WET-map could be used to assess the RSP computation in a comparison with the one that could be computed by the treatment planning system. Our experimental validation showed that this kind of comparison can be impacted by residual set-up errors which were mitigated by applying the registration method for proton radiography data proposed by Deffet et al [10].

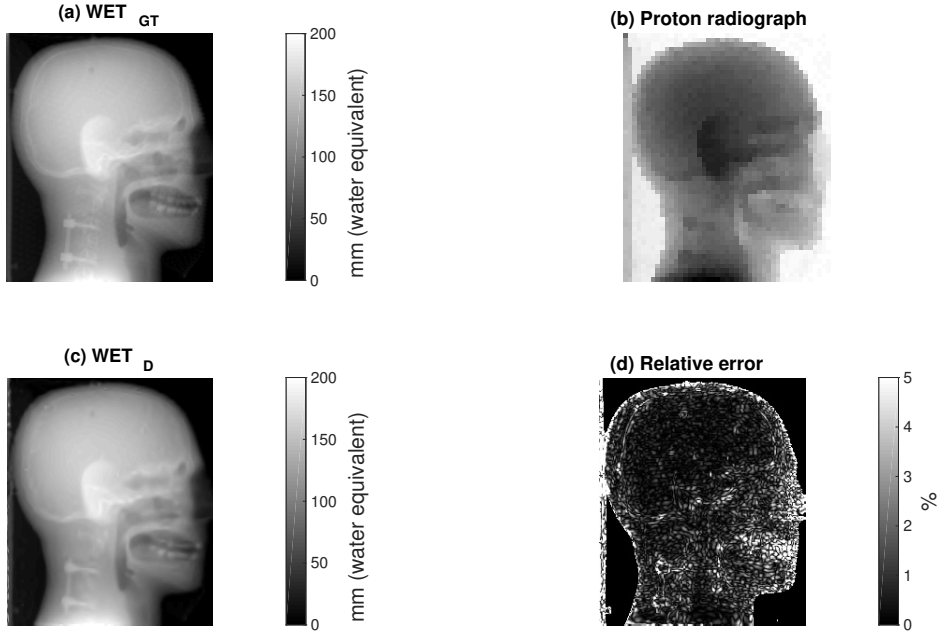

Fig. 2. (a) Ground truth WET, (b) Projection in the form of a range map of the proton radiograph used as input, (c) WET obtained after deconvolution and super-resolution, (d) relative error after deconvolution and super-resolution.

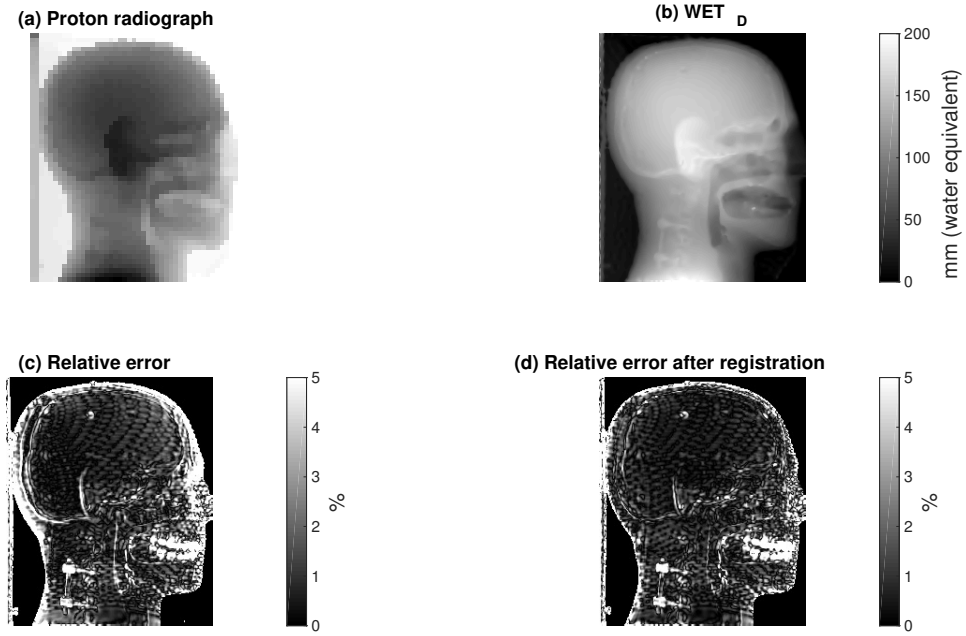

Fig. 3. (a) Projection in the form of a range map of the proton radiograph used as input, (b) WET obtained after deconvolution and super-resolution, (c) Relative error between the WET-map estimated by the treatment planning system and the one obtained by deconvolution and super-resolution of proton radiography data, (d) Relative error after registration.

5. REFERENCES

[1] H Paganetti, "Range uncertainties in proton therapy and the role of monte carlo simulations," *Physics in Medicine Biology*, vol. 57, no. 11, pp. R99, 2012.

[2] I Rinaldi, S Brons, O Jäkel, B Voss, and K Parodi, "Experimental investigations on carbon ion scanning radiography using a range telescope," *Physics in Medicine Biology*, vol. 59, no. 12, pp. 3041, 2014.

[3] P Farace, R Righetto, and A Meijers, "Pencil beam proton radiography using a multilayer ionization chamber," *Physics in Medicine Biology*, vol. 61, no. 11, pp. 4078, 2016.

[4] U Schneider, P Pemler, J Besserer, E Pedroni, A Lomax, and B Kaser-Hotz, "Patient specific optimization of the relation between ct-hounsfield units and proton stopping power with proton radiography," *Medical Physics*, vol. 32, no. 1, pp. 195–199, 2005.

[5] P J Doolan, M Testa, G Sharp, E H Bentefour, G Royle, and H-M Lu, "Patient-specific stopping power calibration for proton therapy planning based on single-detector proton radiography," *Physics in Medicine Biology*, vol. 60, no. 5, pp. 1901, 2015.

[6] C-A Collins-Fekete, S Brousmiche, D C Hansen, L Beaulieu, and J Seco, "Pre-treatment patient-specific stopping power by combining list-mode proton radiography and x-ray ct," *Physics in Medicine Biology*, vol. 62, no. 17, pp. 6836, 2017.

[7] M Mumot, C Algranati, M Hartmann, J M Schippers, E Hug, and A J Lomax, "Proton range verification using a range probe: definition of concept and initial analysis," *Physics in Medicine Biology*, vol. 55, no. 16, pp. 4771, 2010.

[8] N Krah, M Testa, S Brons, O Jäkel, K Parodi, B Voss, and I Rinaldi, "An advanced image processing method to improve the spatial resolution of ion radiographies," *Physics in Medicine Biology*, vol. 60, no. 21, pp. 8525, 2015.

[9] P Farace, R Righetto, S Deffet, A Meijers, and F Vander Stappen, "Technical note: A direct ray-tracing method to compute integral depth dose in pencil beam proton radiography with a multilayer ionization chamber," *Medical Physics*, vol. 43, no. 12, pp. 6405–6412, 2016.

[10] S Deffet, B Macq, R Righetto, F Vander Stappen, and P Farace, "Registration of pencil beam proton radiography data with x-ray ct," *Medical Physics*, vol. 44, no. 10, pp. 5393–5401, 2017.

[11] D. Pflugfelder, J. J. Wilkens, H. Szymanowski, and U. Oelfke, "Quantifying lateral tissue heterogeneities in hadron therapy," *Medical Physics*, vol. 34, no. 4, pp. 1506–1513, 2007.